Atmospheric oxidation of 4-(2-Methoxyethyl) phenol initiated by OH radical in the presence of O_2 and NO_x: A mechanistic and kinetic study

Junfang Yao[1], Yanan Sun[1], Yizhen Tang[2], Yunju Zhang[3], Wenzhong Wu[4], Jingyu Sun[1*]

[1] *Hubei Key Laboratory of Pollutant Analysis & Reuse Technology*, *College of Chemistry and Chemical Engineering, Hubei Normal University, Cihu Road 11, Huangshi, Hubei, 435002, P. R. China*

[2]*School of Environmental and municipal Engineering, Qingdao University of Technology , Fushun Road 11. Qingdao, Shandong, 266033, P.R. China.*

[3]*Key Laboratory of Photoinduced Functional Materials, Mianyang Normal University, Mianyang, Sichuan, 621000, P. R. China*

[4]*College of Foreign Languages, Hubei Normal University, Cihu Road 11, Huangshi, Hubei 435002, P. R. China*

Abstract: 4-(2-Methoxyethyl) phenol (MEP), a significant methoxypheolic compound, plays an important role in the formation of secondary organic aerosols (SOA). The present work focuses on the gas-phase oxidation mechanism and kinetics of MEP with OH reaction by the density functional theory (DFT). Energetically, favourable reaction channels and feasible products were identified. The initial

[1]* Corresponding author. Email address: sunjy@hbnu.edu.cn Tel.:; Fax: 0714-6515602

reactions of MEP with OH radical produces two different channels: OH addition and H abstraction. Subsequent reaction schemes of the main intermediates in the presence of O_2 and NO_x are investigated through using quantum chemical methods at M06-2X/6-311++G(3df,2p)//M06-2X/6-311+G(d,p) level. Ketene, diketones and nitrophenol compounds are demonstrated to be dominant oxidation products. The total and individual rate constant are calculated by using the traditional transition state (TST) theory at 298K and 1atm. The calculated value of 1.69×10^{-11} cm^3 $molecule^{-1}$ s^{-1} is close to experimental data. Moreover, the lifetime of MEP is estimated to be 16.4 hours. These results provide a comprehensive explanation for atmospheric oxidation pathways of MEP and show that MEP would be removed by OH radical in the atmosphere.

Keywords: 4-(2-Methoxyethyl) phenol, OH radical, DFT, reaction mechanism, rate constants, lifetime

1.Introduction

Biomass of woods, crops, and wastes has always been recognized as one of the important fuels for cooking and heating. Usually, biomass burning emissions will emit a multitude of greenhouse gas such as CO_2, CO and hydrocarbons, other air pollutants such as SO_2, NO_x, volatile organic components(VOCs), and smoke particles bringing carcinogenic substances[1-3]. With increasing usage of biomass fuels, the issue of

climate change, global warming and their negative impacts on human health have been brought to the public attentions. Some earlier studies showed that woodsmoke exposure can lead to many adverse health effects, such as acute respiratory infections, tuberculosis, asthma, chronic obstructive pulmonary disease, lung cancer[4]

Commonly, woody biomass combustion would generate the emission of particular matter ($PM_{1\text{-}10}$). Some studies indicated that wood smoke are enriched more than 70% of PM2.5 and PM10 in residential areas[5,6]. Thus, it is evident that the wood combustion has a significant impact on air quality. Generally, the wood biomass includes different components, mainly consisting of cellulose, hemicelluloses and lignin[7]. A large number of methoxyphenols are created by the combustion of lignin, and the rate of the emission of methoxyphenols from the pyrolysis of lignin is about 900-4200mg/kg[8-10]. if so, the concentration of methoxyphenols in atmospheric environment reaches to several thousand nanograms per cubic meter. Methoxyphenols as semi-volatile organic compounds are distributed between gas and particle phases. However, many of methoxyphenols were discovered to have higher percentages in the gas phase than in the particle phase by the measument of distribution[11]. Therefore, the methoxyphenols have determined the contribution of wood smoke to atmospheric environment pollution. The studies of the atmospheric mechanism of methoxyphenols are particularly important for understanding of their effects on the atmosphere. To our knowledge, there are many removal processes to eliminate methoxyphenols in the atmosphere, such as wet and dry sedimentation, direct photolysis and radical reactions for example hydroxyl, chlorine and nitrate. Methoxyphenols in aerosols generally undergo chemical transformation by heterogeneous reactions such as absorbing on graphene or aqueous-phase radical reactions[12-15]. More notably, for the elimination of methoxyphenols in the gas-phase, the hydroxyl radical should be the main responsibility during the day.

Methoxyphenols mainly consist of methoxyphenols (2-methoxyphenol (guaiacol), 2,6-dimethoxyphenol (syringol)) and their derivatives. The atmospheric degradation processes for guaiacol and syringol with OH radicals have been investigated in experimentally and theoretically[16-19]. For example, Coeur-Tourneur and Lauraguais et al. have researched the OH-initiated reactions of methoxyphenols early in a simulation chamber, The rate constants at 294 ± 2 K and atmospheric mechanism involved guaiacol, creosol and syringol have been given [14,20,21]. However, one of their derivatives, 4-(2-Methoxyethyl) phenol (MEP), has not been well characterized for gas-phase removal processes. He et al. have measured rate constant k_{298K} = (1.7 ± 0.4) × 10^{10} L mol^{-1} s^{-1}(($(2.8\pm0.4)\times10^{-11}$ cm^3 $molecule^{-1}$ s^{-1}) for MEP with OH-initiated in the aqueous[15] . In order to forecast the most favorable reaction pathway of MEP reaction with the OH radical in each mechanism, the frontier electron density (FED)[22,23] of carbon atoms on the aromatic ring and the hydrogen-bond dissociation energy (BDEs)[24] of O-H/C-H bonds in the substitute groups were calculated via using the quantum chemical method. The structure of MEP has been drawn in Figure 1. In their study, both C2 and C6 atoms have the maximal FED of 0.023 in MEP, which explains that the OHaddition mostly takes place at carbon positions next to the OH group. The BDEs of O11-H12, C13-H14/H15, C16-H17/H18 and C20-H21/H22/H23 bonds were calculated as 356, 363, 386 and 394 kJ mol^{-1}, respectively. It was found that the BDE of O11-H12 was the lowest. As a result, the most favorable H-abstraction pathway is from OH group. FEDs and BDEs can only predict the possible reaction sites for the addition and abstraction of MEP initiated by OH radical. Whereas, literature didn't really provide the detailed reaction mechanisms and subsequent reactions.

In the present work, we conducted a computational study on OH-initiated gas-phase reaction of MEP in the presence of O_2 and NO by using density functional

theory(DFT). In order to determine the energetically favourable reaction pathways and dominant products, the energy barrier and thermodynamic parameters have been calculated. Rate constants of initial degradation of MEP have been also constructed. We expect the present work could be a supplement to experimental study and further understand the behavior of mehtoxyphenols in the atmosphere.

2. Computation Details

All of the quantum chemical calculations were performed by using the Gaussian09 suit of program[25]. In the present work, all the reactants(R), transition states(TS), intermediates(IM) and products(P) were optimized by the M06-2X[26] hybrid meta exchange-correlation functional in conjunction with the 6-311+G(d,p) basis set. The choice of theoretical method, M06-2X, was based on previous computational studies on methoxyphenols[27-29] and the M06-2X has been recommended because of its accurate results such as thermochemical and kinetic data[30-32]. Harmonic frequency analyses were calculated at the same level to distinguish initial conformation obtained whether they were true minimal or first-order saddle points. The minimal were identified with zero imaginary frequency. And the transition states were optimized to ensure a single imaginary vibration frequency, which were confirmed by vibrations analyse and intrinsic reaction coordinate (IRC) [33,34] calculations. In addition, single-point energies were calculated by using M06-2X method at the more accurate 6-311++G(3df,2p) basis set and the reaction potential energy surfaces were constructed at the above-mentioned level. All of possible reaction pathways involved in the OH-initiated degradation of MEP were discussed. The corresponding energies obtained by M06-2x/6-311++G(3df,2p) level were used

to the following discussions.

All calculations for the rate constants of elementary reactions in this work have been performed by conventional Transition State Theory (TST)[35-37]. The TST rate constant has been conducted by:

$$k^{TST} = \sigma \frac{k_B T}{\mathrm{h}} \left(\frac{RT}{P_0} \right)^{\Delta \mathrm{n}} \mathrm{e}^{-\Delta \mathrm{G}^{0,\neq} / k_B T}$$

Where σ, k_b, h and T are reaction path degeneracy, Boltzmann constant, and Planck's constant and temperature, respectively. $\Delta G^{0,\neq}$is the free energy barrier including the thermodynamic contribution corrections. Δn is 1 or 0 for bimolecular or unimolecular reactions. RT/P_0 has the units of inverse concentration.

3. Results and Discussion

3.1 Reaction of MEP with OH radical

For the convenience of the following discussion and analysis, the geometric structures of important reactants, complexes, transition states, stable intermediates and products of initial reactions are displayed in Figure 2. Similar to guaiacol, creosol and syringol, the primary reaction pathways of OH radical with MEP exist two reaction types: OH addition and hydrogen abstraction. Six nonequivalent OH addition could be produced, and eight kinds of pathways are involved in the H abstraction.

Therefore, six different addition products could be created through addition of OH to C1, C2, C3, C4, C5 and C6 atoms of aromatic ring in MEP molecule. The corresponding potential energy surfaces are drawn Figure 3. The potential barriers of addition of OH radical to C1-C5 of aromatic ring are about 0.31-1.23 kcal/mol. However, when OH radical is added to C6 position of aromatic ring, the lowest energy consumption is -2.35 kcal/mol. Apparently, the negative barriers are symbol of

existence of per-reaction complex for TS6. Reliably, there exists a complex which is 4.84 kcal/mol lower than reactants, named RCa. In RCa, the position of OH radical parallels to the benzene ring of MEP molecule, and the oxygen atom of OH group points to H atoms linked to benzene ring C6, forming intra-molecular hydrogen bonds with a bond length of 2.377Å. By analyzing the potential energy surface of MEP with OH addition, it is found that the process of forming IM6 is the main addition path. Compared with IM6, the above five addition pathways (IM1-IM5) are less important so that they are not be further discussed.

The corresponding potential energy surfaces for H atom abstraction in MEP have been depicted in Figure 3. Since the electron density of aromatic ring in MEP is large and the C-H binding force is also strong, the H atom on aromatic ring is difficult to be abstracted, H abstraction pathway from C2-H,C3-H,C5-H,C6-H at 298K and 1atm have potential barriers in the range from 1.30 to 3.25 kcal/mol. While the energy barriers of H atom abstracting from on $-CH_2CH_2OCH_3$ and -OH fragment are essentially -1.67 to 0.32 kcal/mol. And we can see that energy barriers of HTS2 (H loss from $-CH_2$ next to the methoxy group) and HTS6 (H loss from -OH) are -1.67 and -1.39 kcal/mol. Therefore, the negative energy value can be attributed to the presence of pre-reactive complexes. According to the intrinsic reaction coordinates (IRC) calculation, the pre-existing complexes are determined, named RCb and RCc, which are -5.36 and -4.90 kcal/mol lower in potential barriers than reactants, respectively. The difference of potential barriers suggests that the hydrogen abstraction pathways *via* HTS2 and HTS6 to generate IM8 and IM12 are dominant.

3.2 Subsequent reaction of intermediate IM6

3.2.1 Reaction of IM6 with O_2

The OH adding IM6 in initial reaction is an activated radical in the atmosphere and they can react with O_2 preferentially. The potential energy diagram of IM6 with

O_2 reactions is depicted in Figure 4. The O_2 addition reaction can occur at the both sides of the aromatic ring, leading to the formation of four peroxy radicals named as IM6-1OO*s/a* and IM6-2OO*s/a* (*s/a=syn/anti*). As displayed in Figure 4, O_2 adds at *ortho*-position of OH group, producing IM6-1OO*s/a* through TS7*s* and TS7*a* with energy barriers of -0.45 kcal/mol and 2.94 kcal/mol, respectively. Hence, There exists a pre-reaction complex (RCd) with 10.11 kcal/mol of energy less than IM6 and O_2. It is obvious that the energy barrier through TS7*s* to form IM6-1OO*s* is lower than that through TS7*a* to form IM6-1OO*a*. These discusses suggest that IM6-1OO*s* is a feasible intermediate. In the same way, the reaction channels of IM6-2OO*s/a* and IM6-1OO*s/a* are greatly similar. The calculated results still show that energy barriers from the syn-direction additions are slightly lower than that from the anti-direction, which agrees with the theoretical studies on guaiacol, benzene and toluene[19,38,39]. Consequently, O_2 additions at syn-position to produce IM6-1OO*s* and IM6-2OO*s* are the most feasible pathways and they will be further discussed in their subsequent reactions.

3.2.2Reactions of IM6-1OO*s* and IM6-2OO*s*

In atmospheric environment, IM6-1OO*s* and IM6-2OO*s* may possess three types of subsequent reactions: (I) intra-molecular H-shift; (II) reaction of bicyclic peroxy radicals; (III) bimolecular reaction with NO or HO_2. The subsequent reaction processes of IM6-1OO*s* and IM6-2OO*s* are shown in Figure 5. For IM6-1OO*s,* the intramolecular H-shift reaction happens from the -OH to -OO group *via* five-membered and six-membered ring transition states to construct IM6-1OO*s*-1 and IM6-1OO*s*-2, respectively. Once IM6-1OO*s*-1 is generated, it follows by HO_2-elimination to acquire P1(Ketene). However, the potential energy barrier for H-shift is higher about 22.07 kcal/mol. It indicates that the reaction to generate P1 through this channel is not feasible. Similarly, the energy barrier of the other H-shift pathway is

23.44 kcal/mol. Certainly, two H-shift pathways are hindered. The second type of reaction is ring-closure channel. IM6-1OO*s* peroxy radicals could isomerize to form bicyclic peroxy radicals, the terminal O atom of -OO group could attack C atoms of benzene ring, leading to 4-membered, 5-memered or 6-memered cycle formed by two O atoms and the connected C atoms. Apparently, the O atom of -OO group attacks C5 atoms of the benzene ring to form IM6-1OO*s*-5 with the lowest potential barriers of 10.80 kcal/mol and heat release of 9.46 kcal/mol. So the reaction forming IM6-1OO*s*-5 is the most favorable channel due to its exothermicity and relatively low energy barriers. The last pathway is bimolecular reaction with NO or HO_2. Firstly, one of pathway is abstracting the H-atom of HO_2 to produce hydroperoxide (P3) and O_2. Here, the HO_2 radical is considered in a single state. The formation of hydroperoxide (P3) experiences a high potential barrier (41.35 kcal/mol) and endothermicity (5.30 kcal/mol). It is indicated that it is unlikely to occur in the atmosphere. The another subsequent reactions of the IM6-1OO*s* with NO are expected. The IM6-1OO*s* can undergo NO addition, followed by the elimination of NO_2, leading to the formation of an alkoxy radical IM6-1OO*s*-8 and NO_2. Subsequently, ketene(P1) is formed. What we've seen is P1should be a stable product in the atmosphere as IM6-1OO*s* reacts with NO barrierlessly. And the channel is exothermic by 12.32 kcal/mol. For all the above-mentioned processes of IM6-1OO*s*, ring-closure to produce IM6-1OO*s*-5 is predominant and the formation of ketene (P1) through NO addition is also important.

For IM6-2OO*s*, the subsequent reaction pathways are similar to those of IM6-1OO*s*, the H transfer from-CH_2- and -OH group to the terminal O atom of -OO group results in the formation of IM6-2OO*s*-1 and IM6-2OO*s*-2. The reactions through four-membered-ring and six-membered-ring transition state of TS-IM6-2OO*s*-1 and TS-IM6-2OO*s*-2 are not feasible due to their high potential barriers (32.38-36.78 kcal/mol). Furthermore, four possible bicyclic intermediates are detected, in which

IM6-2OO*s*-5 is an important bicyclic peroxy radicals. IM6-2OO*s* connected with HO_2 show less important in the atmospheric oxidation condition owing to high reaction barriers. IM6-2OO*s* still prefers to react with NO only in polluted areas, which would convert to P4 after several elementary reactions.

3.3 Subsequent reaction of intermediate IM8 and IM12

Firstly, IM8 is one of the most favorable intermediate from H abstraction in the initial reaction between OH radical and MEP, which is probable subjected to be further oxidized by O_2/NO_x in atmosphere. The relevant processes of IM8 are depicted in Figure 6. Additions of IM8 with O_2 are both barrierless, releasing larger enthalpy of 73.80 and 86.50 kcal/mol, respectively. O_2-addition product (IM8-OO) can react with NO and HO_2 to complete its further degradation. On the one hand, IM8-OO abstracts H from HO_2 to generate P7 and O_2. The reaction has high potential barrier of 39.58 kcal/mol, suggesting that the pathway plays a less significance role. On the other hand, the peroxy radical IM8-OO can react with NO barrierlessly and produce an unstable peroxy nitrite IM8-OO-1. This addition reaction is exothermic by 10.73 kcal/mol, followed the production of IM8-OO-2 by the elimination of NO_2. Then the alkoxy radical IM8-OO-2 reacts with O_2 would lead to form a stable product P9, and this energy barrier is about 7.83 kcal/mol. In addition, IM8-OO-2 through C-O bond breakage to form the product 2-(4-hydroxyphenyl)acetaldehyde (P8) and -OCH_3 group are not feasible due to their high potential energy (32.38 kcal/mol).

Secondly, Figure 7 summarizes the subsequent reaction pathways of IM12. Likewise, IM12 is the main intermediate of H abstraction, but its subsequent reactions are quite different from IM8. IM12 will first undergo intramolecular double bond transfer to form IM12-1barrierlessly. In the atmosphere, O_2 molecule can directly add at C6 of aromatic ring to form IM12-1OO with large heat release of 59.72 kcal/mol. Later, the intermediate of IM12-1OO can subsequently proceed H-shift, ring-closure

and reaction with HO_2/NO. These reaction pathways are similar to those of IM6-1OO*s*. For example, the reactions through four-membered-ring H-shift transition state of TS-IM12-1OO-1, then diene ketone(P10) is acquired. However, the calculation shows that the H-transfer reactions of IM12-1OO are difficult to occur in the atmosphere due to high energy barrier (36.32 kcal/mol). The cyclization IM12-1OO product would lead to the formation of four-, five- and six-membered ring intermediates. For IM12-1OO, the cyclization is not favorable pathways due to their high potential barriers (23.43~35.32 kcal/mol) and endothermicity (1.77~11.04 kcal/mol). Similarly, abstracting the H atom of HO_2 to form P11 is unfavorable pathway since the high potential barrier is 37.56 kcal/mol. The most feasible pathway is that it reacts with NO to form diene ketone (P10).

3.4 Reaction of IM6, IM8 and IM12 with NO_2

The possible reaction schemes of IM6, IM8 and IM12 with NO_2 are depicted in Figure 8. For IM6, the NO_2 molecule mainly adds to C1 and C3 positions of aromatic ring. In analogy to O_2 addition, the reaction can occur from both *anti/syn*-positions with respect of OH group, leading to form four isomers. Then nitrophenols (P12, P13 and P14) are produced by eliminating H_2O, H_2O_2 and H_2, and all of reactions are exothermic. As discussed above, P12 were identified as the key product of IM6 with NO_2 because IM6-1NO_2*s* releases large heat by eliminating H_2O. For IM8 and IM12, the reaction pathway is also highly exothermic. NO_2 is directly added to IM8 and IM12 resulting in the formation of feasible product P14 and P15.

4. Kinetics calculations

Obviously, the calculations of rate constants and atmospheric lifetimes to the elementary reaction are essential in assessing the transport and fate of methoxyphenols. In my work, the individual and total rate constants for the OH radical reaction with MEP have been calculated by traditional transition state

theory(TST) at 298K based on the M06-2x/6-311++G(3df, 2p)// M06-2x/6-311+G(d, p) energies. The calculated total rate constant for MEP with OH reaction is 1.69×10^{-11} cm^3 $molecule^{-1}$ s^{-1} at 298 K. A comparison between our results and experimental values is unavailable because of lack of experimental data for the reaction of MEP with OH in gas phase. Alternatively, we have chosen the rate constants of congeners with OH reactions for indirect comparison. Coeur-Tourneur et al have determined that rate constants of guaiacol and syringol with OH are $(7.53\pm0.41)\times10^{-11}$ and $(9.66\pm1.11)\times10^{-11}$ cm^3 $molecule^{-1}$ s^{-1}[20], respectively. And previous theoretical results show that the rate constant of creosol with OH radical is 7.80×10^{-11} cm^3 $molecule^{-1}$ s^{-1} at 298.15K in the atmosphere[19]. Comparing the rate constants of these methoxyphenols, the order of magnitude is the same. Therefore, our results are reasonable. In addition, the rate constant calculated is in reasonable agreement with experimental measurement value of $(2.8\pm0.4)\times10^{-11}$ cm^3 $molecule^{-1}$ s^{-1} in aqueous-phase[15]. The reliability of our result is verified again. As shown in the Table 1, IM8 and IM12 via H abstraction pathways are the most beneficial products with the total yield of 55.04%, and OH radical addition C6 atom accounts for 37.06%, which is in agreement with previous energy barriers calculations.

The lifetime of atmospheric MEP determined by OH radical has been calculated with formula:

$$\tau_{OH} = \frac{1}{k_{(OH+MEP)} \times C_{OH}}$$

Where $k_{(OH+MEP)}$ is the total rate constant and C_{OH} is the 12h daytime average OH radical concentration. A literature pointed out that the concentration of OH radical is 1.0×10^6 molecule cm^{-3} in global atmosphere[40]. The atmospheric lifetime is deduced to be 16.4 hours at 298K and 1 atm. Previous theoretical results show that the lifetimes of guaiacol, syringol and creosol with OH radical are 4.27h, 3.56h and

2.98h. The lifetime of four methoxyphenols follows the order: τ(MEP+OH)>τ(guaiacol+OH)>τ(creosol+OH)>τ(syringol+OH). The results indicated that MEP would take 16.4 h to complete degradation in the atmosphere, which is longer than the other three methoxyphenols.

5.Conclusion

In the present article, we used quantum chemical calculation methods to investigate atmospheric oxidation mechanism of MEP by OH radical in presence of O_2/NO_x. The total and individual rate constants were calculated via using traditional transition state theory(TST) at 298K and 1atm, some key conclusions were depicted in the following:

(1) Two channels were studied for the initial reaction including OH addition and H abstraction. The calculated thermodynamic parameters showed that OH radical preferentially added to C6 position of MEP with the lowest energy barrier of -2.35 kcal/mol. For the abstraction reaction, the channels forming IM8 and IM12 were predicted to be favorable.

(2) The subsequent secondary reactions involved intermediates IM6, IM8 and IM12 were analyzed by DFT. They would combine with O_2. For IM6, the important products included P1 and P4, and bicyclic peroxy radical (IM6-1OO*s*-5 and IM6-2OO*s*-5). For IM8 and IM12, the main products are methyl 2-(4-hydroxyphenyl)acetate(P9) and phenyldiketones(P10). In high-NO_x condition, IM6, IM8 and IM12 could lead to the formation of nitrophenol compounds.

(3) The total rate constant calculated for MEP with OH reaction was 1.69×10^{-11} cm^3 $molecule^{-1}$ s^{-1}, which matched well with similar systems at 298K. The lifetimes of

MEP was estimated to be 16.4 hours. The relatively short lifetime for MEP with OH reaction indicated that the transformation of MEP by OH radical was feasible in the atmosphere.

Acknowledgments

This work is supported by the National Natural Science Foundation of China (Nos. 21507027, 21707062, and 41775119).

References

[1] J. M. Chen, C. L. Li, Z. Ristovski, A. Milic, Y. T. Gu, M. S. Islam, S. X. Wang, J. M. Hao, H. F. Zhang, C. R. He, H. Guo, H. B. Fu, B. Miljevic, L. Morawska, P. Thai, Y. F. LAM, G. Pereira, A. J. Ding, X. Huang, U.C. Dumka, Sci. Total. Environ. **2017**, 579, 1000-1034.

[2] M. Ezzati, D. M. Kammen, Environ. Health. Perspect. **2002** ,110, 1057-1068.

[3] E. D. Vicente, C. A. Alves, Atmos. Res. **2018**, 199, 159-185.

[4] A. K.Bølling, J. Pagels, K. E.Yttri, L. Barregard, G. Sallsten, P. E. Schwarze, C. Boman, Part. Fibre Toxicol. **2009**, 6 (2), 1−20.

[5] M. A. Bari, G. Baumbach, B. Kuch, G. Scheffknecht, Atmos. Environ. **2009**, 43, 4722-4732.

[6] W. Maenhaut, R. Vermeylen, M. Claeys, J. Vercauteren, C. Matheeussen, E. Roekens, Sci. Total. Environ. **2012**, 437, 226-236.

[7] A. Tursi, *Biofuel. Res. J.* **2019**, 22, 962-979

[8] J. J. Schauer, M. J. Kleeman, G. R. Cass, B. R. T. Simoneit, Environ. Sci. Technol. **2001**, 35, 1716-1728.

[9] B. R. T. Simoneit, W. F. Rogge, M. A. Mazurek, L. J. Standley, L. M. Hildemann, G. R. Cass. Environ. Sci. Technol. **1993**, 27, 2533-2541.

[10] C. G. Nolte, J. J. Schauer, G. R. Cass, B. R. T. Simoneit, Environ. Sci. Technol. 2001, 35, 1912-1919.

[11]L. R. Mazzoleni, B. Zielinska, H. Moosmüller. Environ. Sci. Technol. **2007**, 41, 2115-2122.

[12] B. Yang, H. X. Zhang, Y. F. Wang, P. Zhang, J. N. Shu, W. Q. Sun, P. K. Ma, Atmos. Environ. **2016**, 125, 243-251.

[13] C. G. Liu, P. Zhang, Y. F. Wang, B. Yang, J. N. Shu, Environ. Sci.Technol. **2012**, 46, 13262-13269.

[14] J. F. Sun, D. D. Han, D. E. Shallcross, H. J. Cao, B. Wei, Q. Mei, J. Xie, J. H. Zhan, M. X. He, Chem. Eng. J. **2020**. 404, 126484.

[15] L. He, T. Schaefer, T. Otto, A. Kroflič, H. Herrmann, J. Phys. Chem. A. **2019**, 123, 7828-7838.

[16] A. Lauraguais, C. Coeur-Tourneur, A. Cassez, K. Deboudt, M. Fourmentin, M. Choël, Atmos. Environ. **2014**, 86, 155-163.

[17] E. Dorrestijn, P. Mulder, J. Chem. Soc., Perkin Trans. **1999**, 2, 777-780.

[18] B. Wei, J. F. Sun, Q. Mei, M. X. He, Comp.Theor. Chem. **2018**, 1129, 1-8.

[19] Y. H. Sun, F. Xu, X. F. Li, Q. Z. Zhang, Y. X. Gu, Phys. Chem. Chem. Phys. **2019,** 21, 21856-21866.

[20] C. Coeur-Tourneur, A. Cassez, J. C. Wenger, J. Phys. Chem. A. **2010**, 114, 11645-11650.

[21] A. Lauraguais, C. Coeur-Tourneur, A. Cassez, A. Seydi. Atmos. Environ. **2012**, 55, 43-48.

[22] K. Fukui, T. Yonezawa, C. Nagata, H. Shingu. J. Chem. Phys. **1954**, 22, 1433-1442.

[23] R. G. Parr, W. T. Yang, J.Am. Chem. Soc. 1984, 106, 4049-4050.

[24] F. D. Vleeschouwer, V. V. Speybroeck, M. Waroquier, P. Geerlings, F. D. Proft, J. Org. Chem. **2008**, 73, 9109-9120.

[25] M. J. Frisch, G. W. Trucks, H. B. Schlegel, G. E. Scuseria, M. A. Robb, J. R. Cheeseman, J. A. Montgomery, Jr. T. Vreven, K. N. Kudin, J. C. Burant, J. M. Millam, S. S. Iyengar, J. Tomasi, V. Barone, B. Mennucci, M. Cossi, G. Scalmani, N. Rega, G.A. Petersson, H. Nakatsuji, M. Hada, M. Ehara, K.Toyota, R. Fukuda, J. Hasegawa, M. Ishida, T. Nakajima, Y. Honda, O. Kitao, H. Nakai, M. Klene, X. Li, J. E. Knox, H. P. Hratchian, J. B. Cross, C. Adamo, J. Jaramillo, R. Gomperts, R. E. Stratmann, O. Yazyev, A. J. Austin, R. Cammi, C. Pomelli, J. W. Ochterski, P. Y. Ayala, K. Morokuma, G. A. Voth, P. Salvador, J. J. Dannenberg, V. G. Zakrzewski, S. Dapprich, A. D. Daniels, M. C. Strain, O. Farkas, D. K. Malick, A. D. Rabuck, K. Raghavachari, J. B. Foresman, J. V. Ortiz, Q. Cui, A. G. Baboul, S. Clifford, J. Cioslowski, B. B. Stefanov, G. Liu, A. Liashenko, P. Piskorz, I. Komaromi, R. L.Martin, D. J. Fox, T. Keith, M. A. Al-Laham, C. Y. Peng, A. Nanayakkara, M. Challacombe, P. M. W. Gill, B. Johnson, W. Chen, M. W. Wong, C. Gonzalez, J. A.

Pople, Gaussian Inc, Pittsburgh, PA, **2010**. GAUSSIAN 09. Gaussian Inc, Pittsburgh, PA.

[26] Y. Zhao, D. G. Truhlar, Theor. Chem. Accounts. **2008**, 120, 215-241.

[27] J. F. Sun, H. J. Cao, S. Q. Zhang, X. Li, M. X. He, RSC Adv. **2016**, 6, 113561-113569.

[28] B. Wei, J. F. Sun, Q. Mei, Z. X. An, X. Y. Wang, M. X. He, Environ. Pollut. **2018**, 243, 1772-1780.

[29] A. M. Priya, S. Lakshmipathi, J. Phys. Org. Chem. **2017**, 30, e3713.

[30] M. H. Keshavarz, K. Esmailpour, M. Zamani, A. G. Roknabadi, Propell. Explos. Pyrot. **2015**, 40, 886-891.

[31] S. R. Hashemi, V. Saheb, Comput. Theor. Chem. **2017**, 1119, 59-64.

[32] F. Y. Bai, S. Ni, Y. Z. Tang, X. M. Pan, Z. Zhao, Sci. Total. Environ. **2020**, 699, 134-190.

[33] C. Gonzalez, H. B. Schlegel, J. Phys. Chem. **1990**, 94, 5523-5527.

[34] C. Gonzalez, H. B. Schlegel. J. Chem. Phys. **1989**, 90, 2154-2161.

[35] A. Galano, J. R. Alvarez-Idaboy. Org. Lett. **2009**, 11, 5114-5117.

[36] H. Eyring. J. Chem. Phys.**1935**, 3, 107-115.

[37] M. G. Evans, M. Polanyi, Trans. Faraday. Soc. **1935**, 31, 875-894.

[38] Y. Li and L. M. Wang, Phys. Chem. Chem. Phys. **2014**, 16, 17908-17917.

[39] D. R. Glowacki, L. Wang and M. J. Pilling, J. Phys. Chem. A, **2009**, 113, 495 5385-5396

[40] S. Gligorovski, R. Strekowski, S. Barbati, D. Vione, Chem. Rev. **2015**, 115, 13051-13092.

Figure Captions

Figure 1. Optimized geometry of 4-(2-Methoxyethyl) phenol at the M06-2X/6-311+G(d, p) level.

Figure 2. Optimized structures with the selected geometrical parameters (distance in Å and angles in degree) of intermediates, complexes, transition states and products involved in the reaction of MEP with OH radical at the M06-2X/6-311+G(d,p) level.

Figure 3. The dominant potential energy curve for reaction of MEP + OH at the M06-

2X/6-311++G(3df,2p)//M06-2X/6-311+G(d,p) level. (a) Hydrogen abstraction paths. (b) C-addition paths.

Figure 4. Profile of the potential energy surface for the reaction of IM6 with O_2 at the M06-2x/6-311++G(3df,2p)// M06-2x/6-311+G(d,p) level.

Figure 5. Secondary reaction schemes of IM6-1OO*s* and IM6-2OO*s* with potential energy ΔE(kcal mol^{-1}) and the Gibbs activation barrier ΔG(kcal mol^{-1}). (a) IM6-1OO*s* reaction pathways. (b) IM6-2OO*s* reaction pathways.

Figure 6. Secondary reaction scheme of IM8 with the potential barriers ΔE(kcal mol^{-1}) and the Gibbs activation barrier ΔG(kcal mol^{-1}).

Figure 7. Secondary reaction scheme of IM12 with the potential barriers ΔE(kcal mol^{-1}) and the Gibbs activation barrier ΔG(kcal mol^{-1}).

Figure 8. Secondary reaction scheme of IM6, IM8 and IM12 with NO_2 at the M06-2X/6-311++G(3df, 2p)//M06-2X/6-311+G(d,p) level with the Gibbs activation barrier ΔG(kcal mol^{-1}).

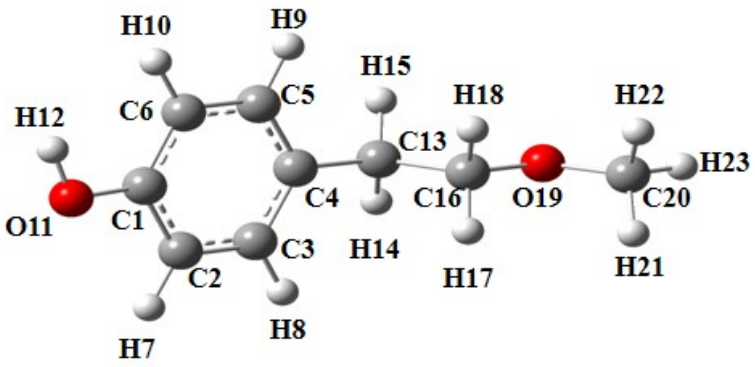
H10
H9
H15
H18
H22
H12
C6
C5
C13
H23
C4
C16
O19
C20
O11
C1
C3
H14
H17
H21
C2
H8
H7

Figure 1.

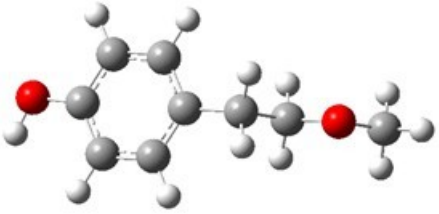

MEP

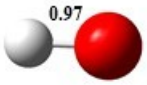

•OH

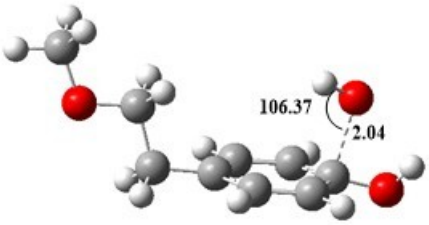

TS1

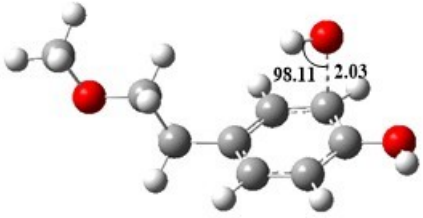

TS2

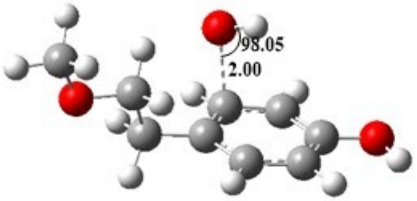

TS3

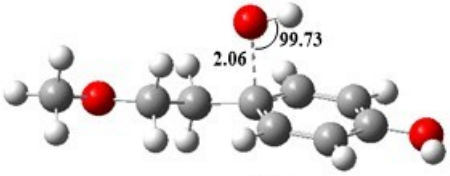

TS4

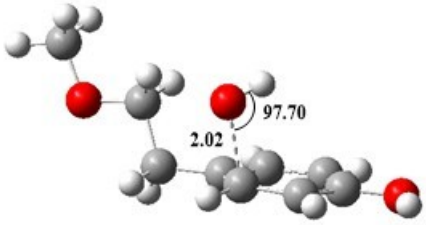

TS5

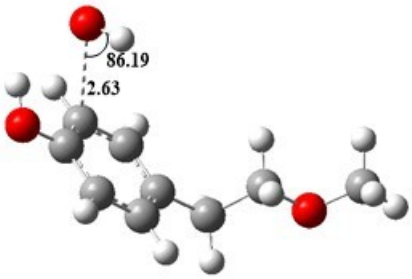

RCa

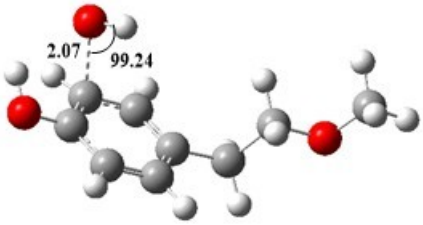

TS6

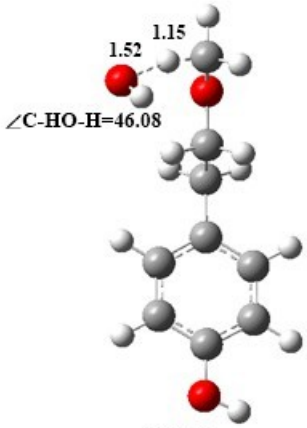

HTS1

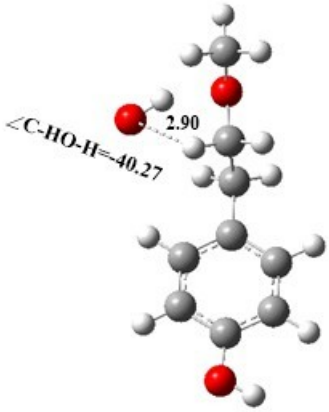

RCb

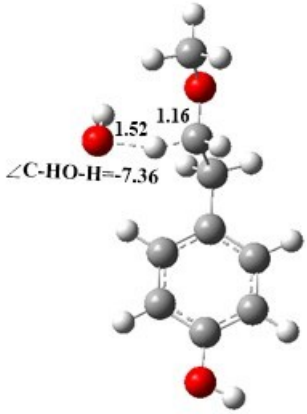

HTS2

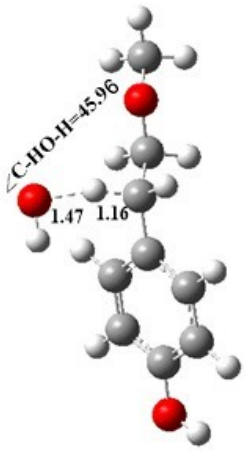

HTS3

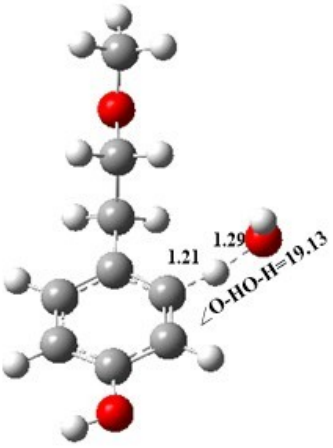

HTS4

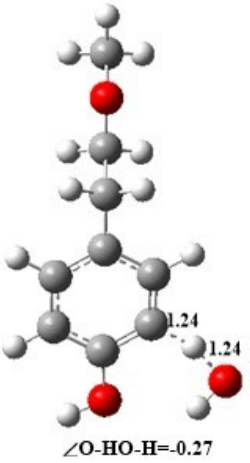

HTS5

RCc

HTS6

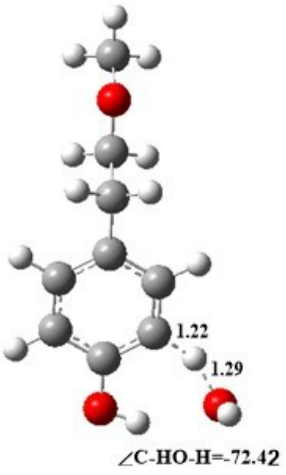

HTS7

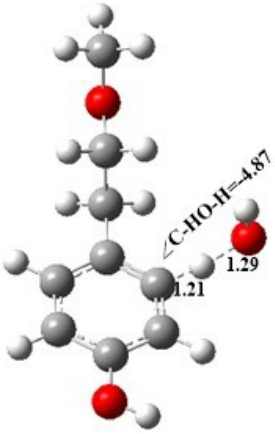

HTS8

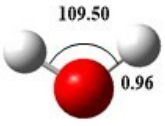

H_2O

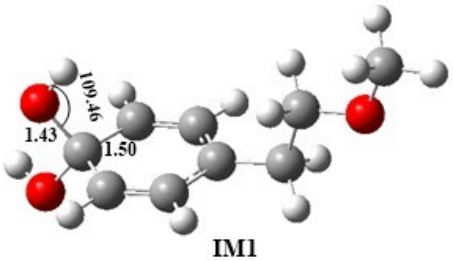

IM1

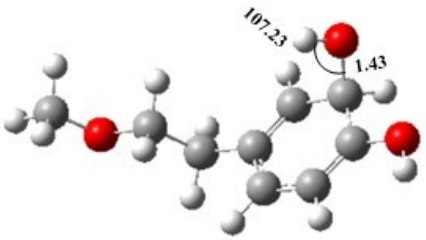

IM2

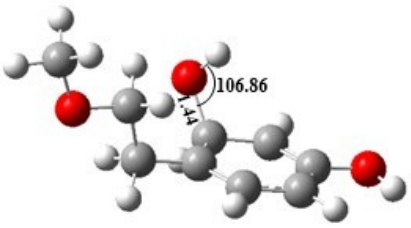

IM3

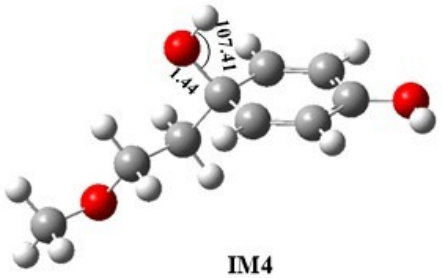

IM4

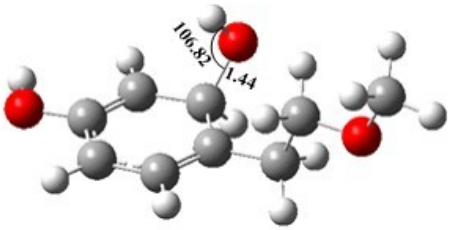

IM5

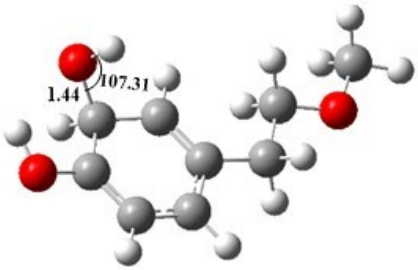

IM6

IM7

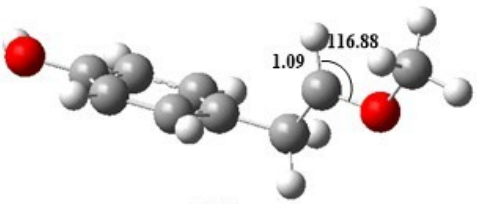

IM8

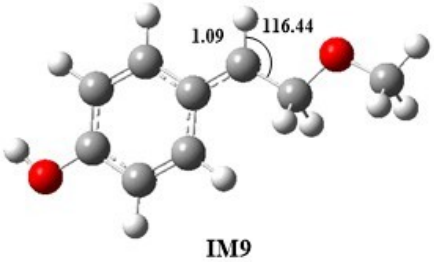

IM9

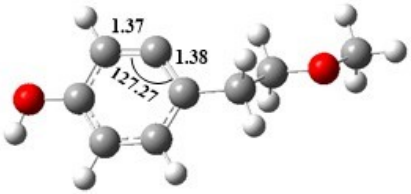

IM10

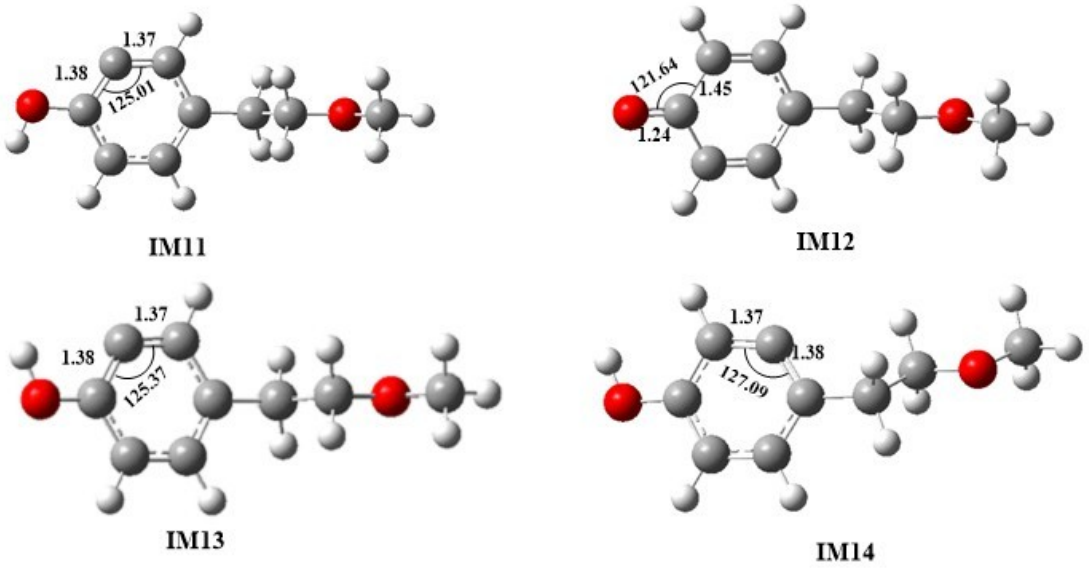
1.37
1.38
125.01
IM11
121.64
1.45
1.24
IM12
1.37
1.38
125.37
IM13
1.37
1.38
127.09
IM14

Figure 2.

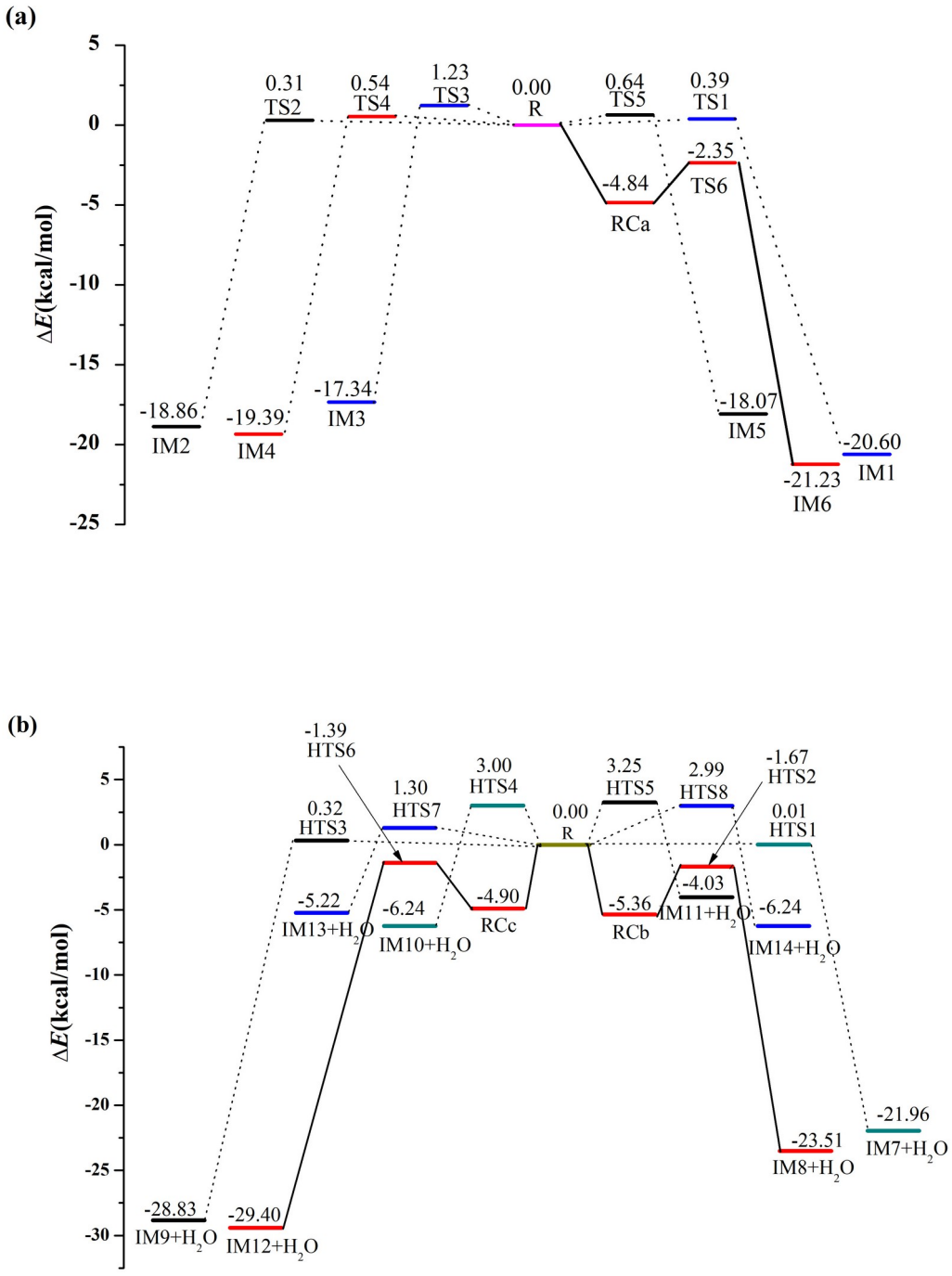
(a)
ΔE(kcal/mol)
5
0
-5
-10
-15
-20
-25
0.31
TS2
0.54
TS4
1.23
TS3
0.00
R
0.64
TS5
0.39
TS1
-2.35
TS6
-4.84
RCa
-18.86
IM2
-19.39
IM4
-17.34
IM3
-18.07
IM5
-20.60
IM1
-21.23
IM6
(b)
ΔE(kcal/mol)
5
0
-5
-10
-15
-20
-25
-30
-1.39
HTS6
0.32
HTS3
1.30
HTS7
3.00
HTS4
0.00
R
3.25
HTS5
2.99
HTS8
-1.67
HTS2
0.01
HTS1
-5.22
IM13+H2O
-6.24
IM10+H2O
-4.90
RCc
-5.36
RCb
-4.03
IM11+H2O
-6.24
IM14+H2O
-28.83
IM9+H2O
-29.40
IM12+H2O
-23.51
IM8+H2O
-21.96
IM7+H2O

Figure 3.

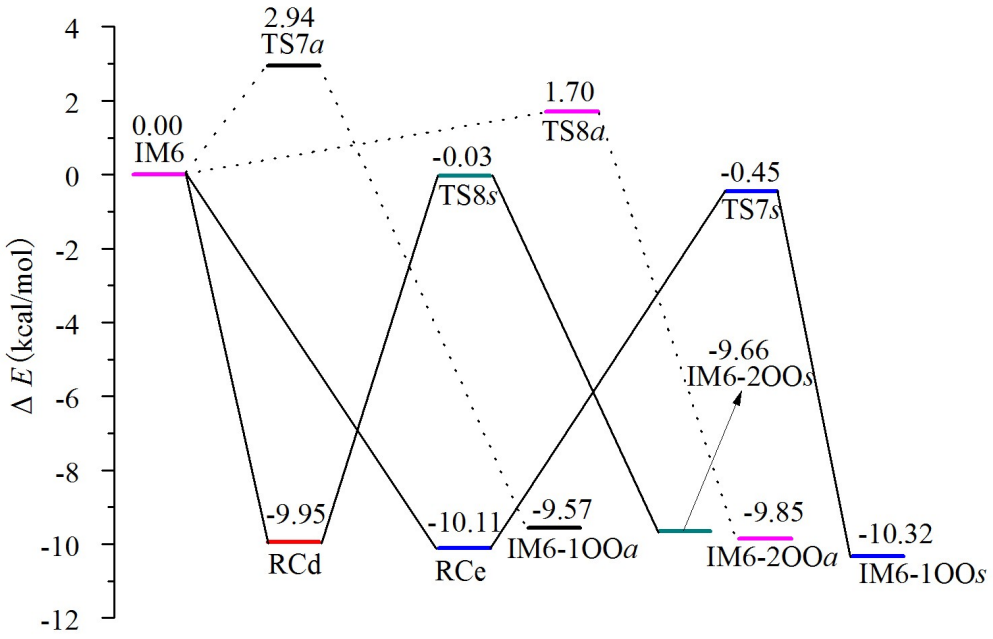
4
2
0
-2
-4
-6
-8
-10
-12
Δ E (kcal/mol)
2.94
TS7a
1.70
TS8a.
0.00
IM6
-0.03
TS8s
-0.45
TS7s
-9.66
IM6-2OOs
-9.95
RCd
-10.11
RCe
-9.57
IM6-1OOa
-9.85
IM6-2OOa
-10.32
IM6-1OOs

Figure 4.

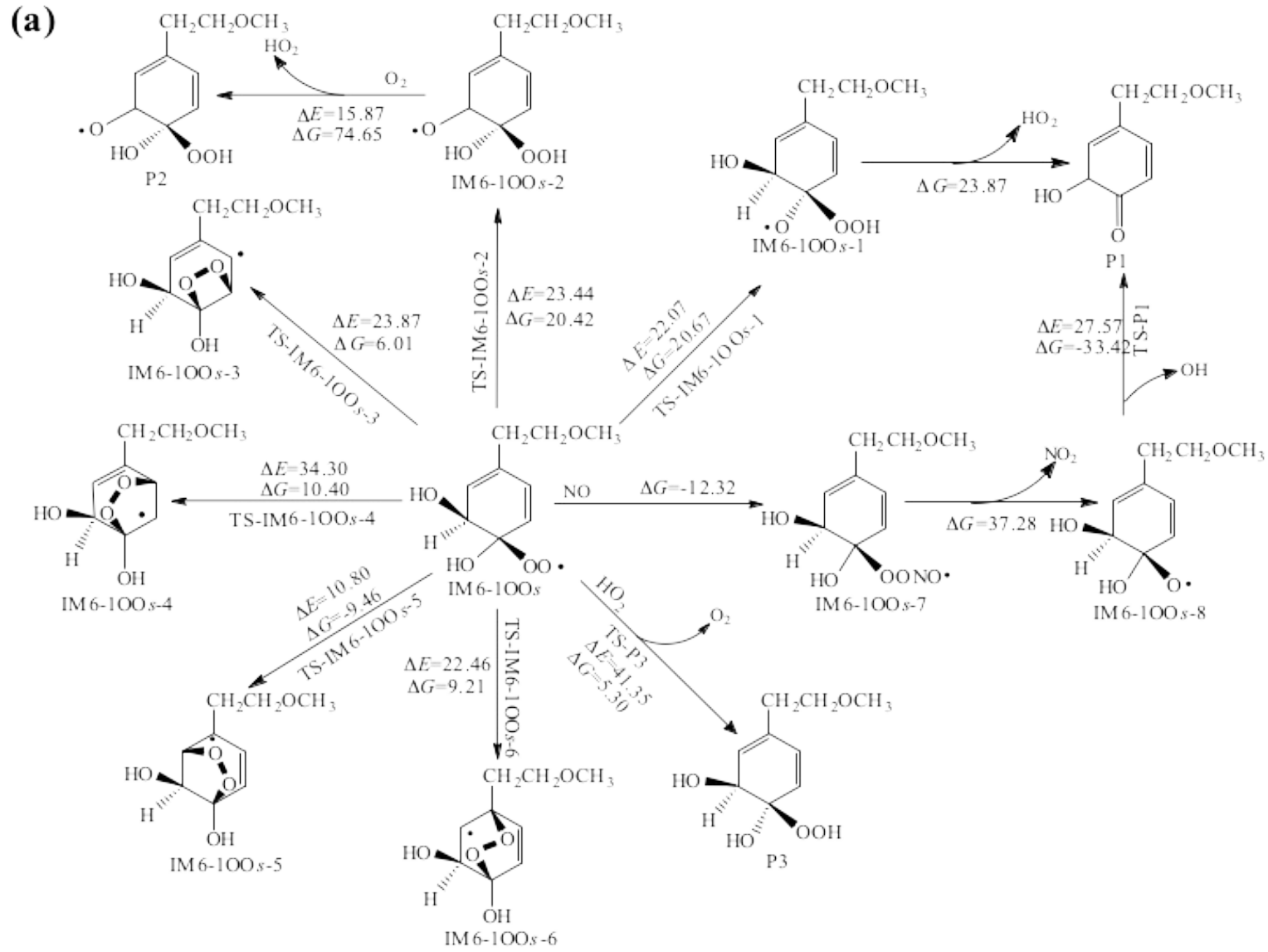
(a)
P2
IM6-1OOs-2
IM6-1OOs-1
P1
IM6-1OOs-3
IM6-1OOs-4
IM6-1OOs
IM6-1OOs-7
IM6-1OOs-8
IM6-1OOs-5
IM6-1OOs-6
P3
ΔE=15.87
ΔG=74.65
ΔG=23.87
ΔE=23.44
ΔG=20.42
TS-IM6-1OOs-2
ΔE=23.87
ΔG=6.01
TS-IM6-1OOs-3
ΔE=22.07
ΔG=20.67
TS-IM6-1OOs-1
ΔE=27.57
ΔG=-33.42
TS-P1
ΔE=34.30
ΔG=10.40
TS-IM6-1OOs-4
NO
ΔG=-12.32
ΔG=37.28
ΔE=10.80
ΔG=-9.46
TS-IM6-1OOs-5
ΔE=22.46
ΔG=9.21
TS-IM6-1OOs-6
TS-P3
ΔE=41.35
ΔG=5.30

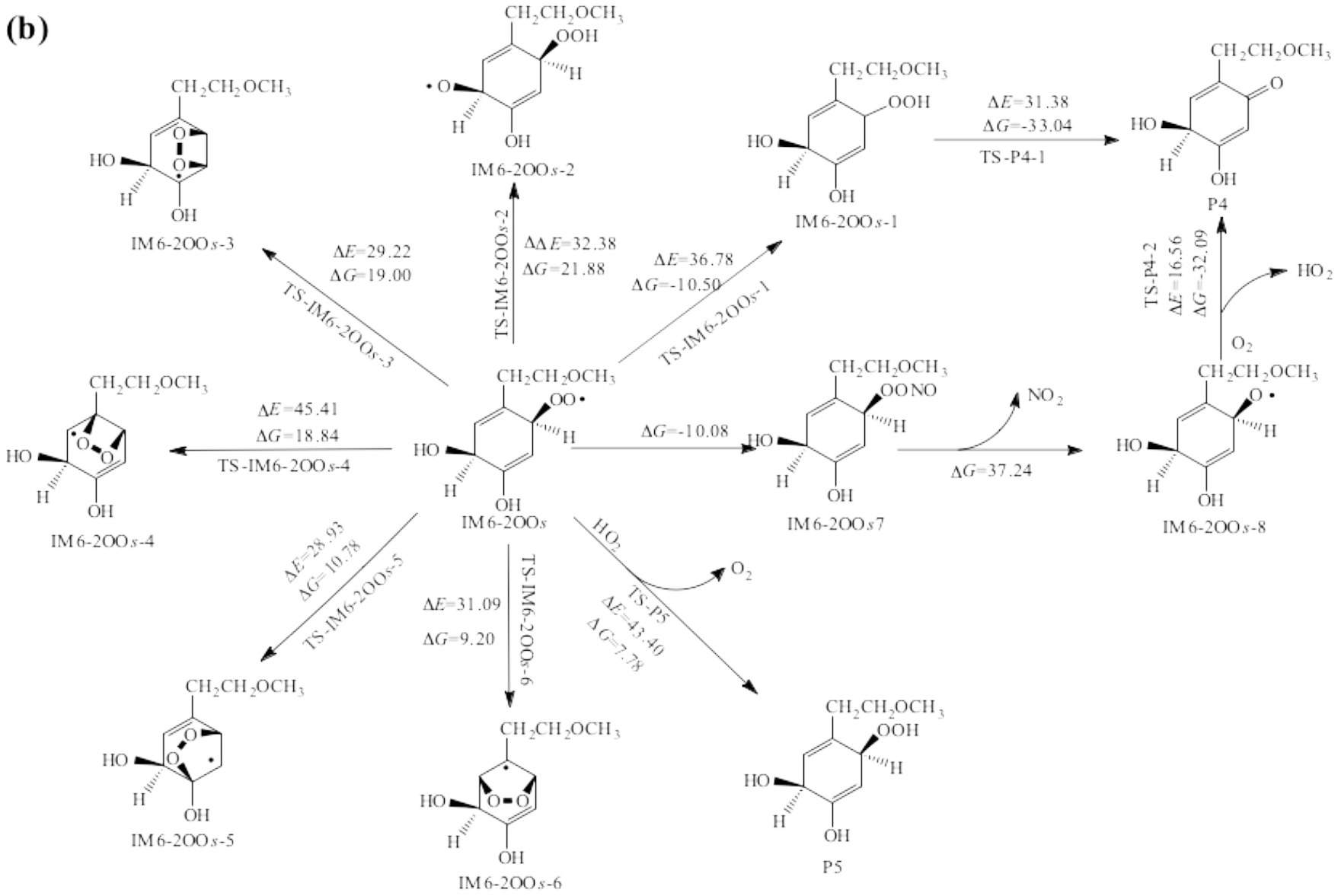
(b)
IM6-2OOs-3
IM6-2OOs-2
IM6-2OOs-1
P4
IM6-2OOs-4
IM6-2OOs
IM6-2OOs7
IM6-2OOs-8
IM6-2OOs-5
IM6-2OOs-6
P5
ΔE=29.22
ΔG=19.00
TS-IM6-2OOs-3
TS-IM6-2OOs-2
ΔΔE=32.38
ΔG=21.88
ΔE=36.78
ΔG=-10.50
TS-IM6-2OOs-1
ΔE=31.38
ΔG=-33.04
TS-P4-1
TS-P4-2
ΔE=16.56
ΔG=-32.09
HO2
O2
ΔE=45.41
ΔG=18.84
TS-IM6-2OOs-4
ΔG=-10.08
NO2
ΔG=37.24
ΔE=28.93
ΔG=10.78
TS-IM6-2OOs-5
ΔE=31.09
ΔG=9.20
TS-IM6-2OOs-6
HO2
TS-P5
ΔE=43.40
ΔG=7.78
O2

Figure 5.

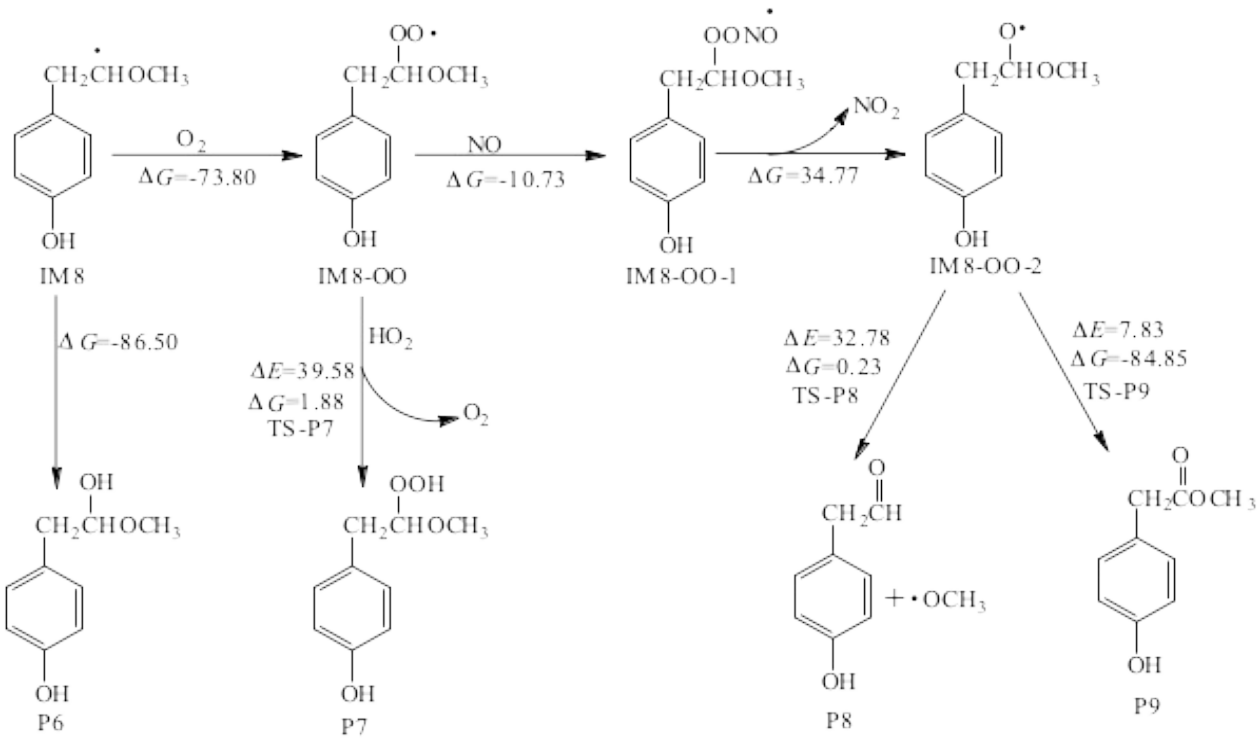
IM8
IM8-OO
IM8-OO-1
IM8-OO-2
P6
P7
P8
P9
ΔG=-73.80
ΔG=-10.73
ΔG=34.77
ΔG=-86.50
ΔE=39.58
ΔG=1.88
TS-P7
ΔE=32.78
ΔG=0.23
TS-P8
ΔE=7.83
ΔG=-84.85
TS-P9

Figure 6.

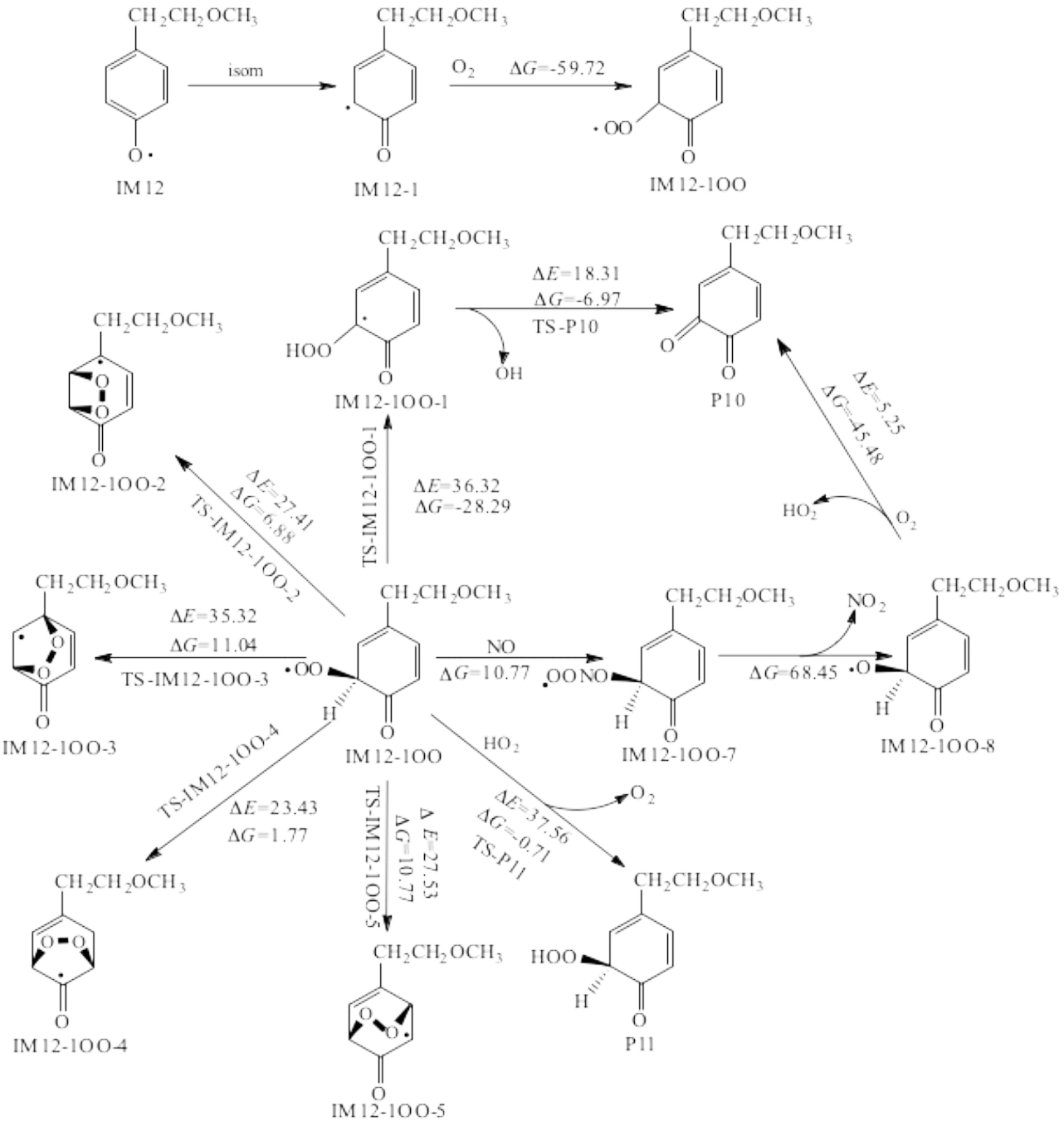
CH2CH2OCH3
isom
O2
ΔG=-59.72
IM12
IM12-1
IM12-1OO
ΔE=18.31
ΔG=-6.97
TS-P10
HOO
OH
IM12-1OO-1
P10
ΔE=5.25
ΔG=-45.48
HO2
O2
IM12-1OO-2
ΔE=27.41
ΔG=6.88
TS-IM12-1OO-2
TS-IM12-1OO-1
ΔE=36.32
ΔG=-28.29
ΔE=35.32
ΔG=11.04
TS-IM12-1OO-3
•OO
NO
ΔG=10.77
•OONO
ΔG=68.45
•O
NO2
IM12-1OO-3
IM12-1OO
IM12-1OO-7
IM12-1OO-8
TS-IM12-1OO-4
ΔE=23.43
ΔG=1.77
TS-IM12-1OO-5
ΔE=27.53
ΔG=10.77
HO2
O2
ΔE=37.56
ΔG=-0.71
TS-P11
IM12-1OO-4
IM12-1OO-5
P11

Figure 7.

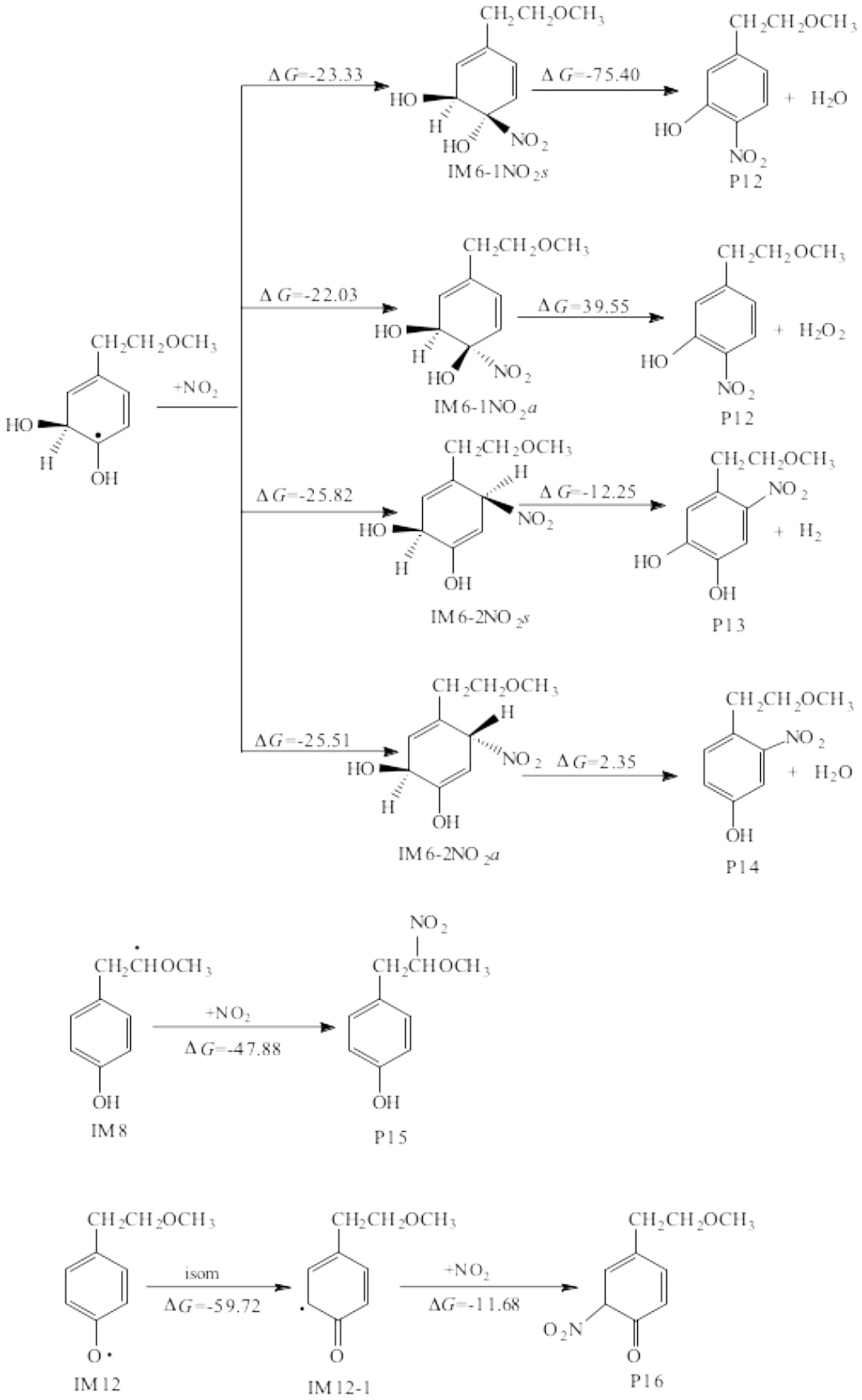
ΔG=-23.33
ΔG=-75.40
IM6-1NO2s
P12
ΔG=-22.03
ΔG=39.55
IM6-1NO2a
P12
+NO2
ΔG=-25.82
ΔG=-12.25
IM6-2NO2s
P13
ΔG=-25.51
ΔG=2.35
IM6-2NO2a
P14
+H2O
+H2O2
+H2
ΔG=-47.88
IM8
P15
isom
ΔG=-59.72
ΔG=-11.68
IM12
IM12-1
P16

Figure 8.

Table 1: Total and individual rate constant k (cm^3 $molecule^{-1}$ s^{-1}) and branching ratio R for the reaction of MEP with OH radical at 298k and 1atm.

Reaction	k	R(%)
MEP+OH→Product	1.69×10^{-11}	100
MEP+OH→IM1	2.99×10^{-14}	0.18
MEP+OH→IM2	2.83×10^{-13}	1.67
MEP+OH→IM3	8.44×10^{-15}	0.05
MEP+OH→IM4	9.04×10^{-15}	0.053
MEP+OH→IM5	2.76×10^{-14}	0.16
MEP+OH→IM6	4.57×10^{-12}	27.00
MEP+OH→IM7+H_2O	2.40×10^{-12}	14.18
MEP+OH→IM8+H_2O	3.05×10^{-12}	17.98
MEP+OH→IM9+H_2O	2.64×10^{-13}	1.56
MEP+OH→IM10+H_2O	1.53×10^{-15}	0.009
MEP+OH→IM11+H_2O	1.16×10^{-15}	0.00
MEP+OH→IM12+H_2O	6.28×10^{-12}	37.06
MEP+OH→IM13+H_2O	3.17×10^{-15}	0.019
MEP+OH→IM14+H_2O	1.37×10^{-14}	0.081